Magnesium Technology 2013

Wrought Materials I

FLOW BEHAVIOR AND HOT WORKABILITY OF PRE-EXTRUDED AZ80 MAGNESIUM ALLOY

Lei Gao[1], Alan A. Luo[2], Shiyi Wang[3], Xiaoqin Zeng[3]

[1]General Motors China Science Lab, 56 Jinwan Road, Pudong, Shanghai 201206, China
[2]General Motors Global Research and Development Center, Warren, MI, USA
[3]National Engineering Research Center of Light Alloy Net Forming, Shanghai Jiao Tong University, Shanghai 200240, China

Keywords: Magnesium alloy, Hot deformation, Processing map, Dynamic recrystallization, Flow instability

Abstract

The hot deformation behavior of pre-extruded AZ80 magnesium alloy has been studied using the processing map technique. Compression tests using Gleeble-3800 thermal simulator were performed in the temperature range of 250-450°C and the strain rate range of 0.001-10 s^{-1}. The flow stress data were used to develop processing maps at true strains of -0.1 to -0.8 according to the well-known dynamic material model and instability criterion. A single dynamic recrystallization (DRX) domain occurs in the range of 420-450°C and 0.1-1.0 s^{-1}, which are the optimum forming conditions for the hot working of this alloy. There are two flow instability regimes occurring at 250-450°C and 0.004-10 s^{-1} and 433-450°C and 0.002-0.014 s^{-1}. The former occurs at low temperatures and/or high strain rates and is associated with adiabatic shear bands or cracks, flow localization, and deformation twinning, while the latter at higher temperatures and lower strain rates is due to abnormal grain growth and wedge cracking.

Introduction

While high-pressure die casting is the dominant process for current magnesium automotive applications, wrought magnesium and their manufacturing processes are receiving increasing attention from academia and industries due to their higher strength and ductility than the cast counterparts [1]. However, wrought magnesium alloys have much less workability than steel or aluminum, especially at low temperatures (<300°C), due to the hexagonal close-packed crystal structure of magnesium [1, 2]. AZ80 (Mg-8.5Al-0.5Zn-0.2Mn, wt.%) is a typical magnesium alloy used in forging and extrusion with high strength, good plasticity and toughness, and good corrosion resistance [3]. The aim of the present investigation is to study the hot workability of AZ80 alloy using the processing map technique and metallography to explore its potential for automotive applications. The optimum temperature-strain rate windows for manufacturing and the flow instability regimes are identified.
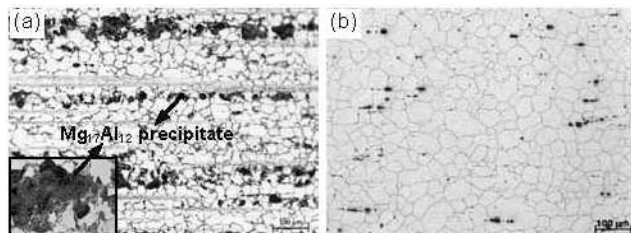

Fig. 1. Micrographs showing the as-extruded (a) and homogenized (b) microstructures of AZ80 alloy. Extrusion direction is horizontal.

The basis for the processing map of a material is the dynamic materials model (DMM) [4], where the workpiece undergoing hot deformation is considered to be a dissipater of power. The strain rate sensitivity (m) of flow stress is the factor that partitions power between deformation heat and microstructural changes. The efficiency of power dissipation, a dimensionless parameter η, occurring through microstructural changes is derived by comparing the non-liner power dissipation occurring instantaneously in the work-piece with that of a linear dissipater for which the m value is unity, and is given by [5]:

$$\eta = \frac{2m}{m+1} \tag{1}$$

The power dissipation map is obtained by plotting iso-efficiency contours of the parameter η in a temperature-strain rate frame at a constant strain. A continuum instability criterion [6, 7] based on the extreme principles of irreversible thermodynamics as applied to large plastic flow [8, 9] is used to identify the regimes of flow instabilities. According to the criterion, flow instability will occur during hot deformation if:

$$\xi(\dot{\varepsilon}) = \frac{\partial \ln[m/(m+1)]}{\partial \ln \dot{\varepsilon}} + m < 0 \tag{2}$$

The variation of instability parameter $\xi(\dot{\varepsilon})$ with deformation temperature and strain rate constitutes an instability map which delineates regimes of instability where ξ is negative.

A superimposition of the instability map on the power dissipation map constitutes a processing map. Processing maps help in identifying temperature-strain rate windows for hot working where the intrinsic workability of the materials is a maximum (e.g. DRX, DRV, and superplasticity) and also in avoiding the regimes of flow instabilities (e.g. adiabatic shear bands or flow localization) [10, 11]. The processing map technique has been used earlier to study the hot deformation mechanisms in pure Mg [12] and Mg alloys [9, 13-16].

Experimental procedure

Pre-extruded commercial AZ80 billets 63 mm in diameter obtained from Magnesium Elektron North America were used as the initial material in this study. The chemical composition of the alloy billets is shown in Table 1. The billets were homogenized at 400°C for 24 h before machining the specimens for workability testing.

Table 1. Chemical composition of AZ80 alloy (in wt.%).

Alloy	Al	Mn	Zn	Fe	Ni	Cu	Zr	Y	Mg
AZ80	7.8	0.14	0.26	<0.01	<0.01	<0.01	<0.01	<0.01	Balance

Cylindrical specimens 10 mm diameter and 15 mm tall were machined from the billets with their longitudinal axis parallel with the pre-extrusion direction. Uniaxial compression testing for hot workability analysis was carried out using a Gleeble-3800 machine at a constant strain rate ranging from 0.001 to 10 s^{-1} and

at an initial temperature between 250 and 450°C. The specimens were heated at a rate of 2°C/s and soaked for 3 min at the preset temperature in low vacuum to allow the temperature to equalize throughout the specimen. Graphite flakes were used as the lubricant in all the experiments. The specimens were deformed up to a true strain of -1.0 (height reduction ~63%) and rapidly quenched into water. The true stress-strain (σ_T-ε_T) curves were derived from the nominal stress-strain (σ_N-ε_N) curves obtained in compression according to the following formulas: $\sigma_T=\sigma_N(1+\varepsilon_N)$, $\varepsilon_T=\ln(1+\varepsilon_N)$. The processing maps were developed according to Eqs. (1) and (2). Selected samples were deformed to different final true strains of -0.2 and -0.5.
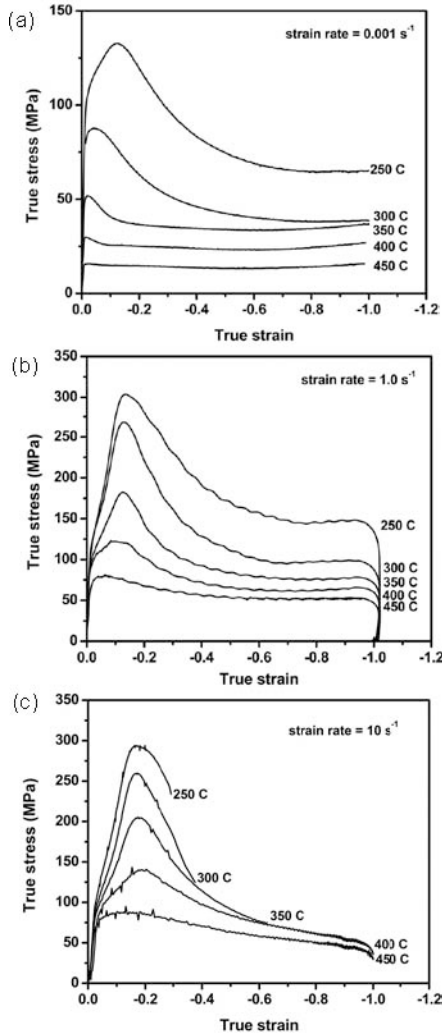

Fig. 2. Typical true stress-true strain curves of AZ80 magnesium alloy at different strain rates and temperatures. (a) 0.001 s^{-1}, 250-450°C; (b) 1.0 s^{-1}, 250-450°C; (c) 10 s^{-1}, 250-450°C.

For metallographic examination, the initial and deformed specimens were sectioned parallel to the compression axis and the cut surfaces were prepared for microstructure observation. Microstructures were observed by optical microscopy (OM) and scanning electron microscopy (SEM). Samples were etched with a solution of 150 ml H$_2$O, 1 g oxalic acid, 1 ml HNO$_3$, and 1 ml acetic acid for 15-30 s. The microscopy was constrained to the central part of the section parallel to the compressive direction.

The average grain size (d) was determined using the mean linear intercept method, where $d = 1.74L$; L is the linear intercept size.


Fig. 3. Macro pictures of the AZ80 samples compressed to ε = -1.0 at 10 s^{-1} and 250-450°C showing shear fracture (T≤ 350 °C) and cracks (400-450°C).

Results and discussion

Initial microstructure

The as-received and homogenized microstructures are shown in Fig. 1. The as-extruded microstructure (Fig. 1(a)) consists of recrystallized fine grains and lamellar β-Mg$_{17}$Al$_{12}$ precipitates (black particles) along deformation bands. It is evident that the precipitates are dissolved into the magnesium matrix after homogenization (Fig. 1(b)), which is in accordance with the Mg-Al phase diagram [17]. The homogenized grain size for AZ80 is about 59 μm (Fig. 1(b)).
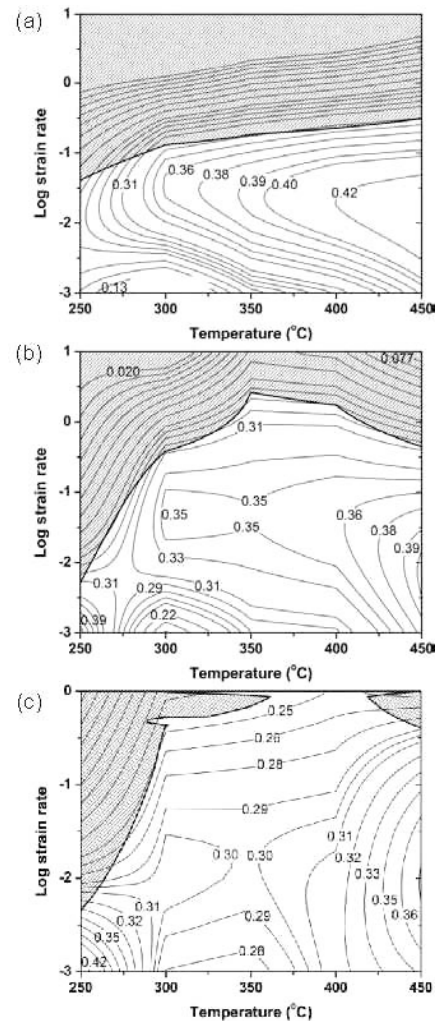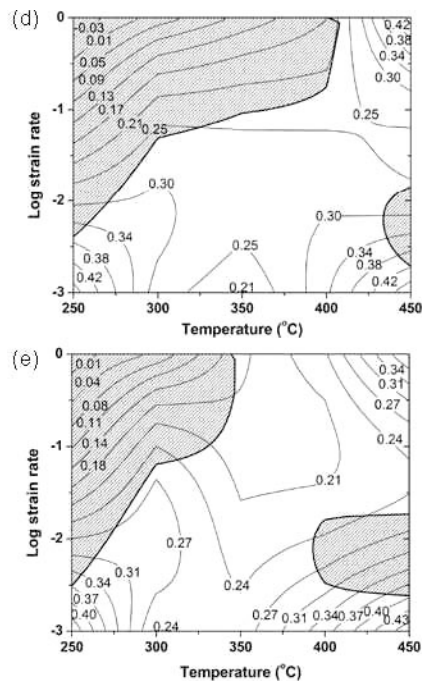
Fig. 4. Processing maps of AZ80 magnesium alloy at true strains of: (a) ε = -0.1, (b) ε = -0.2, (c) ε = -0.3, (d) ε = -0.5, and (e) ε = -0.8. The efficiency of power dissipation (η value) is marked against each contour. The shaded regions correspond to flow instability (ξ < 0). Note the difference in the strain rate range (vertical axis) between (a, b) and (c-e).

Flow stress behavior

Fig. 2 shows the corresponding true stress and true strain curves of AZ80 specimens deformed at 0.001, 1.0, and 10 s^{-1} and at different temperatures. The flow curves (Figs. 2(a) and (b)) at lower strain rates ($\dot{\varepsilon} \leq 1.0$ s^{-1}) show three stages of strain hardening with a single peak, strain softening, and a steady state as strain increases. However, at a higher strain rate of 10 s^{-1} (Fig. 2(c)), the flow behavior is distinctly different and exhibits severe work hardening followed by continuous flow softening. At T $\leq$ 350°C, fracture occurs before or (shortly) following the peak stresses of the curves. All specimens deformed at the strain rate of 10 s^{-1} exhibit shear fracture or cracks, as shown in the macro pictures of the compressed samples in Fig. 3. This type of cracking may be triggered by the onset of intense flow instabilities [18], which is subsequently supported by the processing maps of the AZ80 magnesium alloy.

Processing maps and microstructural interpretation

Fig. 4 shows processing maps of AZ80 alloy obtained at true strains of -0.1, -0.2, -0.3, -0.5, and -0.8. The numbers against the contours represent the efficiency of power dissipation (η value) and the shaded regions correspond to flow instability (ξ < 0). Due to premature failure of the material (Fig. 3), the stress-strain curves at a strain rate of 10 s^{-1} are not well defined to delineate the processing map at strains of ε > -0.2. Note the difference in the strain rate range (vertical axis) between Figs. 4(a)-(b) and 4(c)-(e).
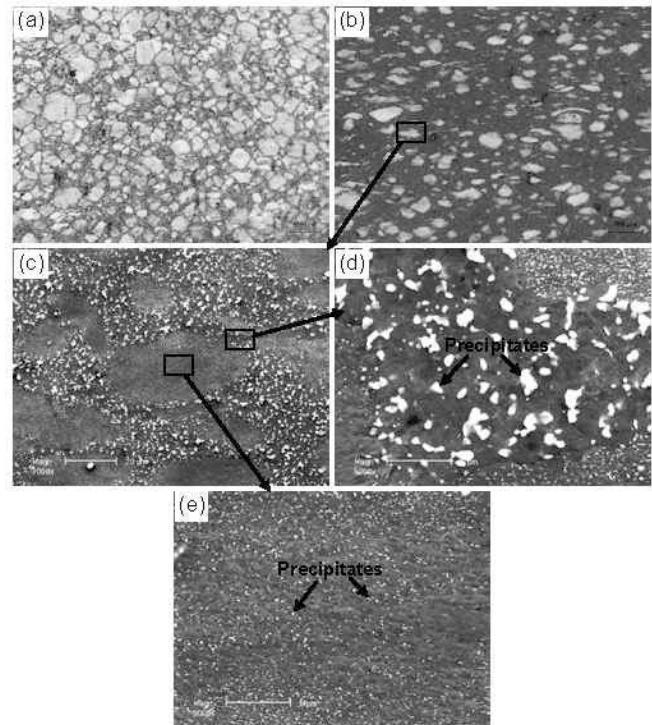

Fig. 5. Optical (a-b) and SEM (c-e) images of AZ80 specimens deformed to ε = -0.5 (a) and ε = -1.0 (b-e) at 250°C and 0.001 s^{-1} showing strain induced precipitates (light particles).

At a strain of -0.1 (Fig. 4(a)), the map exhibits a single domain in the temperature range of 300-450°C and in the strain rate range of 0.003-0.03 s^{-1} with a peak efficiency of 44% occurring at 450°C and 0.01 s^{-1} (*Domain I*). As the strain is increased to -0.2 (Fig. 4(b)), this domain is retained, but with a slight decrease in peak efficiency of power dissipation. In addition, a new domain appears at 250-270°C and 0.001-0.003 s^{-1} with a peak efficiency of 40% occurring at 250°C and 0.001 s^{-1} (*Domain II*). With further deformation to a strain of -0.3 (Fig. 4(c)), *Domain I* is noted to shift to high temperatures T$\geq$ 400 °C, and finally disappears at a strain of -0.5 (Fig. 4(d)). Two new domains appear: one in the range of 420-450°C and 0.1-1.0 s^{-1} with a peak efficiency of about 47% at 450°C and 1.0 s^{-1} (*Domain III*); and the other with a peak efficiency of about 49% at 450°C and 0.001 s^{-1} (*Domain IV*).
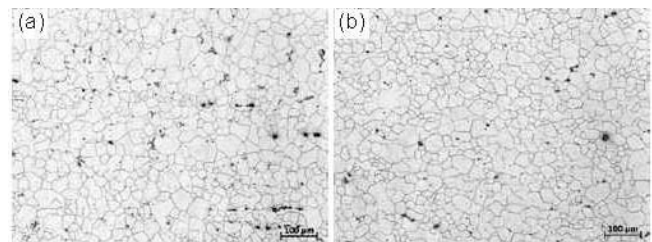

Fig. 6. Optical images of AZ80 specimens deformed to ε = -0.2 (a) and ε = -1.0 (b) at 450°C/1.0 s^{-1} showing fine DRXed grains.

Figs. 5-7 shows the microstructures obtained for specimens deformed at 250°C/0.001 s^{-1}, 450°C/1.0 s^{-1}, and 450°C/0.001 s^{-1}, corresponding to *Domains II-IV*, respectively. Homogenized DRXed grains of ~39 μm are observed in *Domain III* (Fig. 6). However, abnormal grain growth and wedge cracking at grain boundaries occur in *Domain IV* (Fig. 7) due to lower rates of

123

deformation at high temperatures [19]. Grain-boundary sliding is a possibility at lower strain rates and causes wedge cracking which could, in turn, also dissipate energy with high efficiency [4]. No evident DRX is observed in the case of *Domain II*, as shown in Fig. 5. In contrast, a large amount of $Mg_{17}Al_{12}$ particles discontinuously precipitate near the initial grain boundaries, which may also dissipate energy with high efficiency.
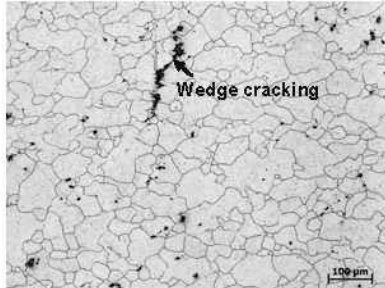

Fig. 7.   Optical image of AZ80 specimens deformed to ε = -1.0 at 450°C and 0.001 s^{-1} showing abnormal grain growth and wedge cracking.

Referring to Figs. 4(a)-(c), AZ80 alloy exhibits a single regime of flow instability at the start of the plastic deformation:

(1) *Regime I* occurs in the temperature range of 250-450°C and strain rate range of 0.004-10 s^{-1}.

With increasing strain to -0.5 (Fig. 4(d)), *Regime I* is partially replaced by *Domain III*, and a new regime of flow instability appears:

(2) *Regime II* occurs in the temperature range of 433-450°C and strain rate range of 0.002-0.014 s^{-1}.

With further deformation to strains up to -0.8 (Fig. 4(e)), *Regime I* is reduced to temperatures lower than 350°C, while *Regime II* extends to the temperature range of 393-450°C and strain rate range of 0.002-0.018 s^{-1}.
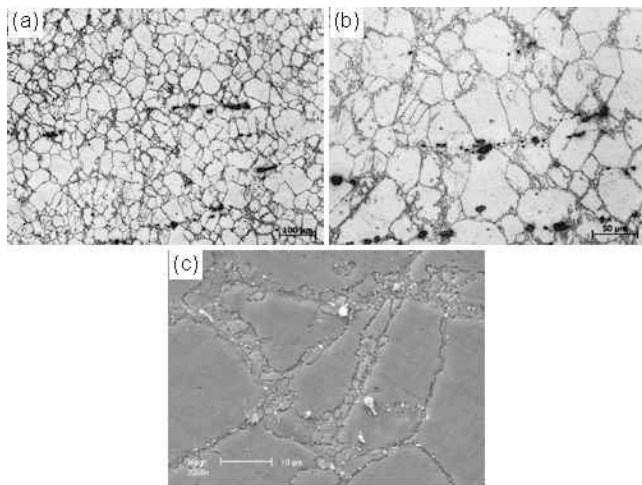

Fig. 8.   Optical (a-b) and SEM (c) images of AZ80 specimens deformed to ε = -0.2 at 300°C and 1.0 s^{-1} showing deformation twinning and DRX at wavy grain boundaries.

Regime I corresponds to the specimens that have undergone shear fracture or cracking (Fig. 3) at the highest strain rate (10 s^{-1}) because of the possible occurrence of adiabatic shear bands [19]. Figs. 8 and 9 show bands of flow localization at 300°C/1.0 s^{-1}

which should be described as unstable deformation regions also corresponding to *Regime I* of flow instability. Due to the limited slip systems at this temperature and a coarse microstructure in the homogenized specimens, many twins occur in the original grains with wavy grain boundaries at the start of deformation, as shown in Figs. 8(a)-(b). DRX and fine precipitates are observed preferentially inside the twins (Fig. 8(c)).

With further deformation to ε = -1.0 (Fig. 9), the compressed sample exhibits highly uneven microstructure, where *Zones A* and *B* are delineated by the red dotted line in Figs. 9(a) and (b). *Zone A* exhibits a similar "necklace" structure to that of Fig. 8, but with a larger fraction of deformation twinning (Figs. 9(c) and (e)). As for *Zone B*, the matrix is crushed by local shear stresses into isolated small blocks (Fig. 9(d)) surrounded by newly formed DRXed grains (Fig. 9(f)). A large number of fine $Mg_{17}Al_{12}$ precipitates are seen to be distributed at the DRXed grain boundaries and play an important role in pinning the DRXed grains from growing. The average grain size is measured to be ~2 μm.
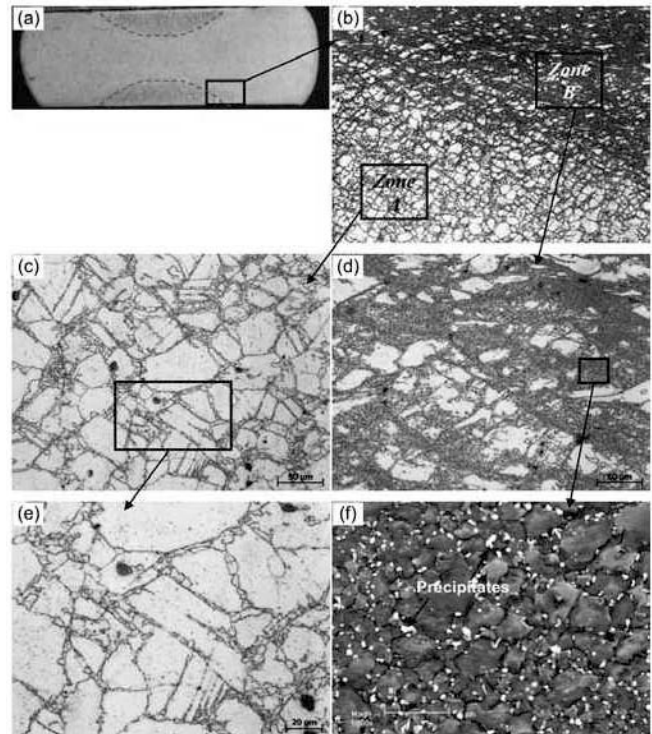

Fig. 9.   Optical (a-e) and SEM (f) images of AZ80 specimens deformed to ε = -1.0 at 300°C and 1.0 s^{-1} showing "necklace" structure and deformation twinning in *Zone A* and shear bands and precipitates in *Zone B*. The red dotted lines in (a) and (b) delineate the interface between *Zones A* and *B*.

Fig. 10 shows the microstructure of the specimen deformed to ε = -1.0 at 450°C and 0.01 s^{-1}, corresponding to *Regime II* of flow instability. Abnormal grain growth (Fig. 10b) and wedge cracking (Fig. 10c) at grain boundaries are detected in the matrix, which are not desirable. Similar microstructures are also observed in *Domain IV* (Fig. 7), which may suggest that *Regime II* extends into *Domain IV* at strain ε > -0.8. These temperatures and strain rates should be avoided in processing the AZ80 alloy.

Conclusions

The processing maps of AZ80 alloy exhibit a single DRX domain in the range of 420-450°C and 0.1-1.0 s^{-1} with a peak efficiency of about 47% at 450°C and 1.0 s^{-1}, which are the optimum forming conditions for the hot working of this alloy. There are two flow instability regimes occurring at 250-450°C and 0.004-10 s^{-1} and 433-450°C and 0.002-0.014 s^{-1}. The former occurs at low temperatures and/or high strain rates and is associated with adiabatic shear bands or cracks, flow localization, and deformation twinning, while the latter at higher temperatures and lower strain rates is due to abnormal grain growth and wedge cracking.
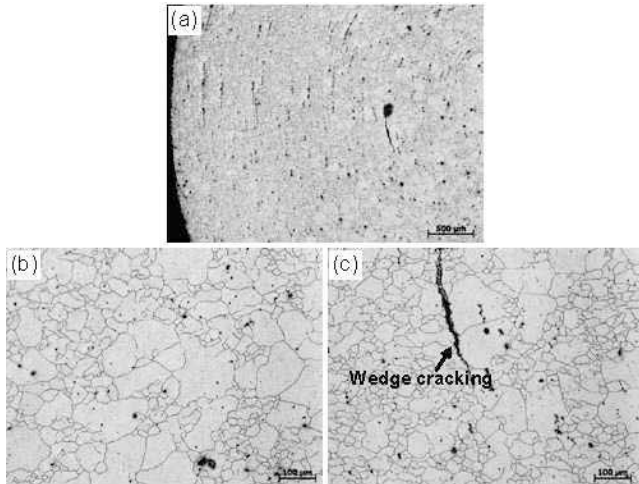

Fig. 10. Optical images (a-c) of AZ80 specimen deformed to ε = -1.0 at 450°C and 0.01 s^{-1} showing abnormal grain growth (b) and wedge cracking (c).

References

[1] A.A. Luo, "Wrought magnesium alloys and manufacturing processes for automotive applications", *SAE Technical Paper*, 2005, no. 2005-01-0734.

[2] Y. Lou, L. Li, J. Zhou, L. Na, "Deformation behavior of Mg–8Al magnesium alloy compressed at medium and high temperatures", *Mater Charact*, 62 (2011), 346-353.

[3] Elektron Wrought Alloys, Magnesium Elektron, http://www.magnesium-elektron.com/.

[4] Y. Prasad, H. Gegel, S. Doraivelu, J. Malas, J. Morgan, K. Lark, D. Barker, "Modeling of dynamic material behavior in hot deformation: Forging of Ti-6242", *Metallurgical and Materials Transactions A*, 15 (1984), 1883-1892.

[5] K.P. Rao, Y.V.R.K. Prasad, K. Suresh, N. Hort, K.U. Kainer, "Hot deformation behavior of Mg-2Sn-2Ca alloy in as-cast condition and after homogenization", *Materials Science and Engineering: A*, 552 (2012), 444-450.

[6] F. Garofalo, "An empirical relation defining the stress dependence of minimum creep rate in metals", *Trans Metall Soc AIME*, 227 (1963), 351-356.

[7] Y.V.R.K. Prasad, "Recent advances in the science of mechanical processing", *Indian J. Technol*, 28 (1990), 435-451.

[8] Y.V.R.K. Prasad, T. Seshacharyulu, "Modelling of hot deformation for microstructural control", *International Materials Reviews*, 43 (1998), 243-258.

[9] J. Luo, M.Q. Li, B. Wu, "The correlation between flow behavior and microstructural evolution of 7050 aluminum alloy", *Materials Science and Engineering: A*, 530 (2011), 559-564.

[10] K.P. Rao, Y.V.R.K. Prasad, N. Hort, K.U. Kainer, "Hot workability characteristics of cast and homogenized Mg-3Sn-1Ca alloy", *J Mater Process Tech*, 201 (2008), 359-363.

[11] H.T. Zhou, Q.B. Li, Z.K. Zhao, Z.C. Liu, S.F. Wen, Q.D. Wang, "Hot workability characteristics of magnesium alloy AZ80-A study using processing map", *Materials Science and Engineering: A*, 527 (2010), 2022-2026.

[12] O. Sivakesavam, I.S. Rao, Y.V.R.K. Prasad, "Processing map for hot working of as cast magnesium", *Mater Sci Tech*, 9 (1993), 805-810.

[13] G.Z. Quan, T.W. Ku, W.J. Song, B.S. Kang, "The workability evaluation of wrought AZ80 magnesium alloy in hot compression", *Materials Design*, 32 (2011), 2462-2468.

[14] X.W. Zheng, A.A. Luo, J. Dong, A.K. Sachdev, W.J. Ding, "Plastic flow behavior of a high-strength magnesium alloy NZ30K", *Materials Science and Engineering: A*, 532 (2012), 616-622.

[15] N. Srinivasan, Y.V.R.K. Prasad, P. Rama Rao, "Hot deformation behaviour of Mg-3Al alloy-A study using processing map", *Materials Science and Engineering: A*, 476 (2008), 146-156.

[16] L. Li, X. Zhang, "Hot compression deformation behavior and processing parameters of a cast Mg-Gd-Y-Zr alloy", *Materials Science and Engineering: A*, 528 (2011), 1396-1401.

[17] T.B. Massalski, P.R. Subramanian, H. Okamoto, L. Kacprzak, Binary alloy phase diagrams, 2nd ed., *ASM International*, Materials Park, OH, 1990.

[18] T. Seshacharyulu, S.C. Medeiros, W.G. Frazier, Y.V.R.K. Prasad, "Hot working of commercial Ti-6Al-4V with an equiaxed α-β microstructure: materials modeling considerations", *Materials Science and Engineering: A*, 284 (2000), 184-194.

[19] S. Anbuselvan, S. Ramanathan, "Hot deformation and processing maps of extruded ZE41A magnesium alloy", *Materials Design*, 31 (2010), 2319-2323.